J Mater Sci (2010) 45:1264–1271
DOI 10.1007/s10853-009-4077-4

Mesoporous titania–silica composite from sodium silicate and titanium oxychloride. Part II: one-pot co-condensation method

Askwar Hilonga · Jong-Kil Kim · Pradip B. Sarawade · Hee Taik Kim

Received: 22 September 2009 / Accepted: 24 November 2009 / Published online: 5 December 2009

Abstract Mesoporous titania–silica composite with large primary particles and homogeneous dispersion of Ti in the silica matrix were synthesized by the sol–gel method via a one-pot co-condensation method using cetyltrimethylammonium bromide (CTAB) as a structure-directing agent. Freshly prepared titanium oxychloride ($TiOCl_2$, titania precursor that is relatively stable) and sodium silicate were used as titania and silica precursors (at the initial ratio of Ti:Si = 1), respectively. The final products were obtained after removing the template by calcination and had overall ratio of Ti:Si = 2:3 (based on EDS and XRF analyses). Other characterization techniques employed include FE-SEM, TEM, FT-IR, DTGA, and nitrogen physisorption studies. The textural properties of the products were highly influenced by the molar concentration of CTAB. Materials with large primary particles (submicrometer-scale dimensions) were obtained at higher concentrations of CTAB (1.7 wt%). The porosities of the templated material were highly reduced compared to that of the untemplated material, emphasizing the influence of Ti loading in the silica matrix. Both pore size and surface area increased at a calcination temperature of 550 °C. The DTGA result showed that the composites exhibited elevated thermal stability (up to 900 °C). In summary, mesoporous titania–silica composite with desirable properties were developed via the proposed method using a relatively inexpensive silica precursor.

Electronic supplementary material The online version of this article (doi:10.1007/s10853-009-4077-4) contains supplementary material, which is available to authorized users.

A. Hilonga · P. B. Sarawade · H. T. Kim (✉)
Department of Chemical Engineering, Hanyang University, 1271 Sa 3-dong, Sangnok-gu, Ansan-si, Gyeonggi-do 426-791, Republic of Korea
e-mail: khtaik@yahoo.com; khtaik@hanyang.ac.kr

J.-K. Kim
E&B Nanotech. Co., Ltd, Ansan-si, Gyeonggi-do, Republic of Korea

Introduction

Several studies have reported the synthesis of titania–silica composites and their enhancement for application in various fields [1–3]. Synthesis of the composites is mainly based on one-pot co-condensation and grafting methods. The former is done by simultaneously reacting the precursors of the composite [4, 5] while the latter is performed by incorporating the guest components into the preformed host's solid network [6]. The one-pot co-condensation method has some merits compared to grafting, because the reacting components are incorporated during the condensation of their frameworks and there are fewer synthesis steps. Given the wide variety of potential applications of titania–silica materials and their application at an industrial scale, there is a need to develop composites with more desirable properties based on precursors that are relatively inexpensive. Most of the reported studies used expensive silica precursors, such as tetraethoxysilane (TEOS), for synthesis of titania–silica composite. Sodium silicate, a relatively inexpensive silica precursor, is used extensively in the synthesis of mesoporous silica (MS, undoped), but has the limitation that materials with large primary particles are rarely produced and few materials have the properties of large surface area and a narrow pore size distribution (PSD), with a few exceptions [7–9]. Furthermore, several studies reporting the synthesis of titania–silica materials do not contain SEM results or those from other characterization techniques suitable for investigating

the morphologies of the materials [10–12], making it impossible to determine the morphologies/sizes of the primary particles in the synthesized products.

Industrial and large-scale production of titania–silica composites is limited by a high-cost conventional precursors, long reaction times (from 1 to 6 days) [13], laborious synthesis steps, and the requirement for hydrothermal treatment [14]. For instance, MS materials have been synthesized using nonionic surfactant and sodium silicate in the pH range from 3 to 10.5 [13]. However, the materials thus obtained have small primary particles between 20 and 50 nm in size. These small particles form spherical agglomerates and combine to form aggregates. The resulting material likely has similar limitations to pure TiO_2 [15]. To the best of our knowledge, there are very few reports on the synthesis of titania–silica composites with large primary particles using sodium silicate as a silica precursor. Composites with large primary particles are in demand because composites with small particles have the following limitations: (a) the small primary particles tend to agglomerate into larger particles, resulting in an adverse effect on catalyst performance (if the final product is to be used as catalyst [15]); (b) The separation and recovery of small particles (e.g., from wastewater) is laborious [16]. Moreover, the use of titanium oxychloride (which has been rarely reported [17, 18]) facilitates the formation of a final product that has desirable properties such as high-purity, an even distribution, and high loading of titania in the composite (probably due to its rapid reaction with silanols and efficient polymerization during the network formation). It is also a relatively stable form of titania precursor which reacts with silica precursor even at lower temperatures (40–60 °C). It should be noted that other titania precursors such as titanium butoxide [$(Ti(OBu)_4$] can only be homogenously dispersed in silica matrix when Si/Ti $\geq$ 10 [19] and in some cases a long hydrothermal treatment time is required for tetrapropylorthotitanate (TPOT) to produce a final product with high titania loading [20].

Kim and Stucky [10] developed a new synthesis method for highly ordered MSs using sodium metasilicate as the silica source and amphiphilic block copolymers as the structure-directing agents. They suggested the incorporation of other substituents such as aluminum or titanium, among others, into the silica framework. Nevertheless, they did not report the morphologies of their final product in their paper (SEM micrographs are missing). Thus, our goal was to develop materials that had all or most of the following desirable properties: large surface area, narrow PSD, definite morphologies and/or large primary particles, and homogeneous dispersion of metal in the silica matrix. In this paper, we report on the synthesis of titania–silica composite materials with large primary particles based on one-pot co-condensation method.

Experimental procedures

Materials

Sodium silicate (24% SiO_2, 7.4% Na_2O) was purchased from Shinwoo Materials Co. Ltd., Republic of Korea. Ammonia solution (28% NH_3), hydrochloric acid (36% HCl), titanium tetrachloride ($TiCl_4$), and cetyltrimethylammonium bromide (98+%CTAB) were purchased from Duksan Chemicals, Republic of Korea.

Synthesis

The preparation of $TiOCl_2$ aqueous solution has been described previously [17, 18]; in this study, we made some modifications as follows: 16.5 mL of reagent grade $TiCl_4$ was dropped slowly in a three-neck flask (inserted in an ice bath) containing 33.5 mL of distilled water. Then, three drops of 1 M HCl was added. The obtained product was labeled as the $TiOCl_2$ stock solution. Because $TiOCl_2$ was freshly prepared and used immediately, all Ti atoms were in monomeric form (this was later confirmed by FT-IR analysis; the vibration bands associated with the presence of –Ti–O–Ti– polymer were not evident). Two experiment sets were performed based on the concentration of CTAB. Since the influence of the various (wide range) concentrations of CTAB on the properties of silica product was already well-documented [7–12], this study was based only on two different concentrations and denoted as low (L) and high (H) concentrations. These CTAB concentrations were sufficient to investigate the influence of the template wt% on the final products developed using the proposed precursors and the suggested synthesis route. Experiment set L was performed as follows: A known amount of CTAB (0.31 g, 0.085 wt%) was dissolved in 30 mL of 2 N HCl solution at room temperature with stirring. After 10 min, 4 g of sodium silicate was added. The sodium silicate was first hydrolyzed for 10 min in this strongly acidic solution. When sodium silicate is hydrolyzed by HCl, silicic acid and NaCl are generated. The Na^+ and CTA^+ act as flocculating agents, as described in the results and discussion section of this study. After 10 min, 10 mL of freshly prepared $TiOCl_2$ solution was added to the hydrolyzed silicate solution to make a molar ratio of Ti:Si = 1. A few drops of ammonia (28%) solution were added after 1 h until gelation was induced (at around pH 6), and the final sol–gel was aged for 2 h. The product obtained was then thoroughly washed with water followed by ethanol and dried at 110 °C for 2 h; this product was referred to as mesoporous titania–silica composite at the low concentration of CTAB (MTSC-XL); where X is the sample number and L is the experiment set/concentration of CTAB. The as-synthesized sample was specifically denoted MTSC-1L. Portions of the

MTSC-1L sample were calcined at temperatures ranging from 550 to 1000 °C for 5 h and labeled MTSC-2L (calcined at 550 °C), MTSC-3L (calcined at 700 °C), and MTSC-4L (calcined at 1000 °C). In experiment set H (high concentration of CTAB, 6.2 g), 1.7 wt% CTAB was used. The samples from this experiment were labeled MTSC-1H, MTSC-2H, etc.

To evaluate the effect of titania loading on the properties of the final product, a similar experiment was conducted in the absence of titania and the product obtained is referred to as MS. The results obtained for this product are discussed briefly under the sub-title "Nitrogen physisorption studies." It should be noted that one of the main advantages of using TEOS as a silica precursor is that all byproducts are volatile, as they are usually alcohols. However, because the precursor employed in this study may leave residues (such as Na^+ and Cl^-) behind in the structure and consequently alter the properties of the material, the as-synthesized materials were first thoroughly washed with water and then rinsed with ethanol. By following this procedure, all byproducts were successfully removed, as assessed using a pH/ISEK Meter (pH-250L, Korea). The purity of the final product was also confirmed by EDS and FT-IR techniques. The experimental procedures reported in this work were repeated three times to examine the reproducibility of the properties of the final products. Generally, no significant differences between the properties of the products obtained from any of the three batches were observed.

Characterization

The morphologies of the titania–silica composite samples were characterized by a scanning electron microscope (FE-SEM, Hitachi, S-4800) with an accelerating voltage of 15 kV. Before performing the FE-SEM characterization, the samples were dried at 110 °C and sprinkled lightly with a spatula on carbon tape with an adhesive surface that was affixed to an aluminum stub. The stub was placed into a sputter coater for 5 min to allow a thin layer of gold to form. The FE-SEM was coupled to an energy dispersive spectroscope (EDS, with a detection limit of 100 ppm and depth resolution up to 3 μm) to assess the purity and elemental composition of the final product. Transmission electron microscope (TEM) micrographs were obtained with a JOEL 2000FX instrument. X-ray diffraction patterns (XRD-6000, Shimadzu) were used to determine the crystallinity of the composite. The accelerating voltage and applied current were 40 kV and 100 mA, respectively. The average crystallite size, D, was calculated using the Debye–Scherrer formula $D = K\lambda/(\beta \cos\theta)$, where K is the Scherrer constant, 0.9; λ is the X-ray wavelength, 1.5406 Å; β is the full width at half-maximum (FWHM) of the diffraction peaks, rad; and θ is the Bragg diffraction angle.

The Brunauer–Emmett–Teller (BET) surface areas and porosities of the samples were studied with a nitrogen adsorption instrument (Micrometrics ASAP 2020). All measured samples were degassed at 250 °C for 1 h prior to the measurements. PSDs and specific desorption pore volumes were determined using the Barrett–Joyner–Halenda (BJH) method. Both adsorption and desorption branches were used to determine PSD. Differential thermogravimetric analysis (DTGA) was performed using a microprocessor-based Parr temperature controller (Model 4846) connected to a muffle furnace (A.H. JEON Industrial Co. Ltd., Korea) at a heating rate of 10 °C/min from room temperature to 1000 °C. The formation of Ti–O–Si bonds in the prepared composites was confirmed using an AVATAR 360 FT-IR (Thermo nicolet). The ratio of Si to Ti was determined using an X-ray fluorescence spectrometer (XRF; XRF-1700, Shimadzu Co., Japan; with a detection limit of 10 ppm and depth resolution up to 10 μm). ZAF corrections (atomic number, Z) were used to determine the molar ratios of the elements present in the composites.

Results

FE-SEM and TEM micrographs

The morphologies of representative samples prepared in this study are shown in Figs. 1 and 2. The samples prepared with 0.085 wt% CTAB had small particles that were loosely aggregated (Fig. 1). Large primary particles with no inter-particle small aggregates formed when 1.7 wt% CTAB was used (Fig. 2). We attribute the observed variation in morphologies between samples to the wt% of CTAB used for synthesis.

XRD patterns

Figure 3 shows the XRD patterns of the composite. The appearance of anatase and rutile peaks confirms the presence of titania particles in the silica matrix. This is also consistent with the EDS and FT-IR results shown in Fig. 4. XRD peaks were assigned to anatase phase titania at 25.3, 37.8, 41.4, 48.0, and 54.5; and to rutile phase titania at 27.5°, 44.1°, and 56.7°.

EDS and FT-IR spectra

No peaks other than those expected for titania–silica composites (Ti, Si, and O) were observed in the EDS spectrum shown as an inset in Fig. 4, indicating the high-purity of the composites obtained in this study. This is consistent with the XRD results presented above as well as the FT-IR results. FT-IR measurements were taken to confirm silica

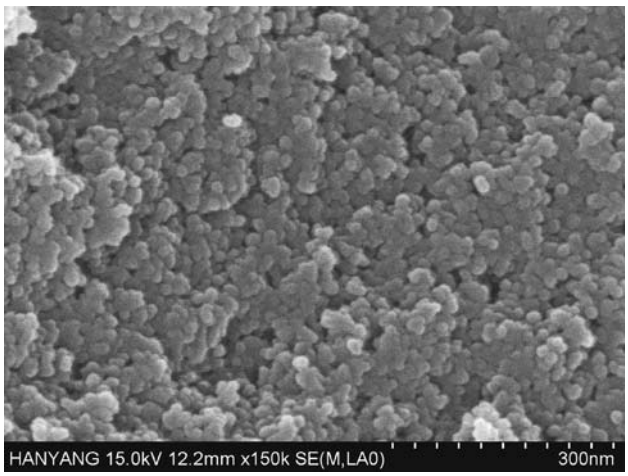

Fig. 1 FE-SEM micrographs of MTSC-3L (at 0.31 g, 0.085 wt% CTAB)

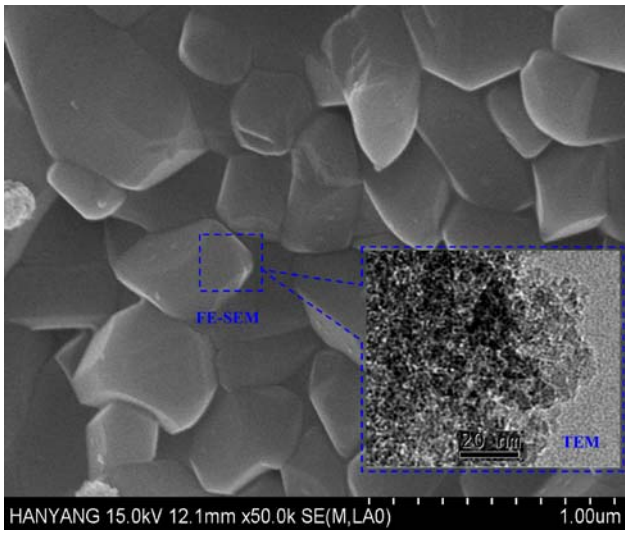

Fig. 2 FE-SEM and TEM (inset) micrographs of MTSC-3H (at 6.2 g, 1.7 wt% CTAB)

formation and the existence of Si–O–Ti bonds (Fig. 4). With reference to previous studies [21], the vibration bands at about 3450 cm^{-1} and 1650 cm^{-1} were attributed to the stretching mode of O–H bonds (hydroxyl group) and water, respectively. The strong bands at 1100 and 472 cm^{-1} were assigned to the asymmetric stretching and bending modes of Si–O–Si, respectively [9]. The peak at 954 cm^{-1} was attributed to the Si–O–Ti vibration band [21].

DTGA Curves

The thermal stability of the composite samples was examined by DTGA curves analyses, and the corresponding curves are available in the supporting information. The obvious peaks observed correspond to the loss of weight due to the evaporation of the remaining water and organic

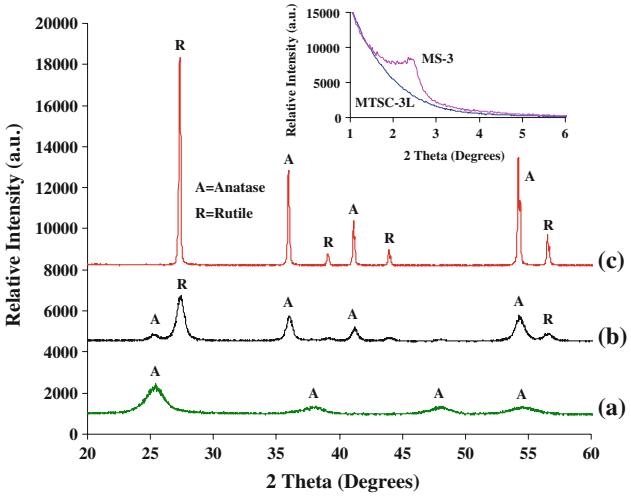

Fig. 3 XRD patterns for the as-synthesized titania–silica composite sample (MTSC-1L) (*a*) together with those calcined at 700 °C (MTSC-3L) (*b*) and 1000 °C (MTSC-4L) (*c*). The inset shows low-angle XRD of MS-3 and MTSC-3L

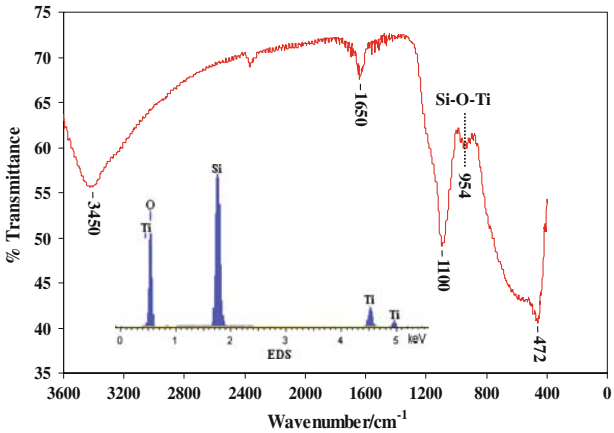

Fig. 4 FT-IR spectrum for MTSC-3L. The inset shows EDS spectra

compounds as well as degradation of the CTAB surfactant. The weight loss at temperatures lower than 250 °C resulted primarily from the removal of physically absorbed water, as reported elsewhere [11]. The loss of weight at 540 °C is due to the degradation of organic matter, i.e., the CTAB template.

Nitrogen physisorption studies

The nitrogen adsorption–desorption isotherms of the prepared samples are shown in Figs. 5 and 6. Generally, the samples exhibited characteristic Type IV curves with capillary condensation steps that signify the presence of mesopores. Characteristic features of Type IV isotherms are a hysteresis loop, which is associated with capillary condensation in mesopores, and limited uptake over a range of high P/P_0 [22]. The initial part of the Type IV

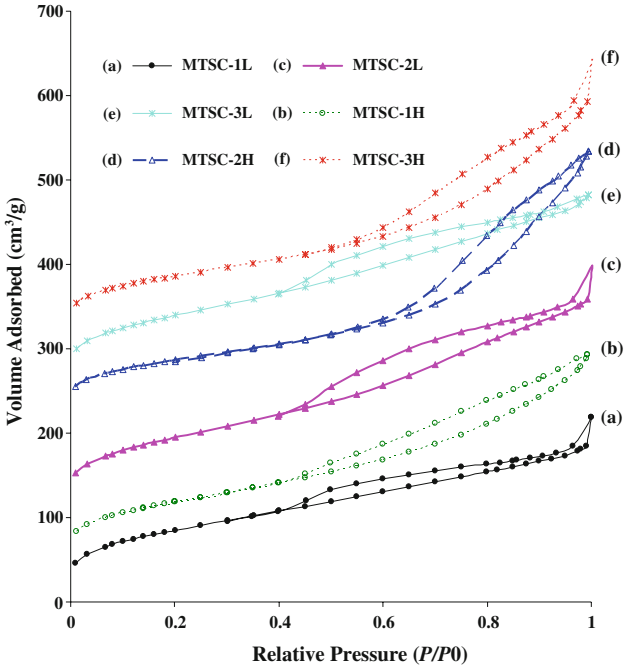

Fig. 5 The nitrogen adsorption–desorption isotherm for *a* MTSC-1L, *b* MTSC-2L, *c* MTSC-3L, *d* MTSC-1H, *e* MTSC-2H, and *f* MTSC-3H samples. To improve the clarity (to separate them), the isotherms have been offset by a constant specific volume of 50 cm^3/g

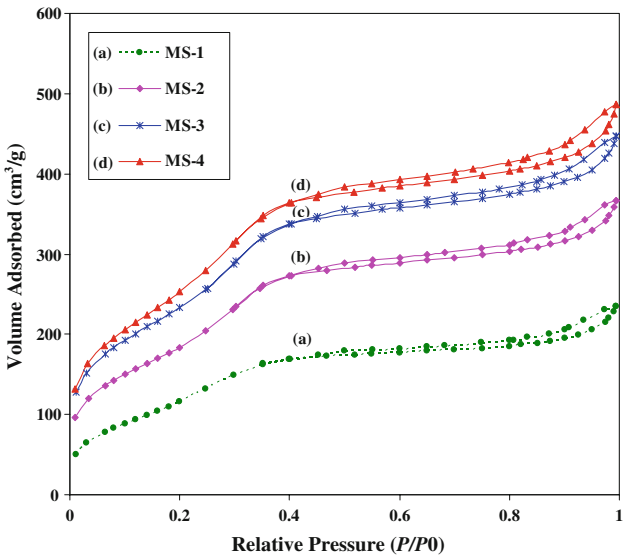

Fig. 6 The nitrogen adsorption–desorption isotherm for *a* MS-1 (as-synthesized), *b* MS-2 (calcined at 550 °C), *c* MS-3 (calcined at 700 °C), and *d* MS-4 (calcined at 1000 °C)

isotherm is attributed to monolayer–multilayer adsorption. The samples calcined at higher temperatures (e.g., MTSC-3H) had Type H3 loops and did not exhibit limiting adsorption at high P/P_0. This is attributed to the presence of aggregates of plate-like particles that gave rise to slit-shaped pores. In contrast, the MS samples possessed Type

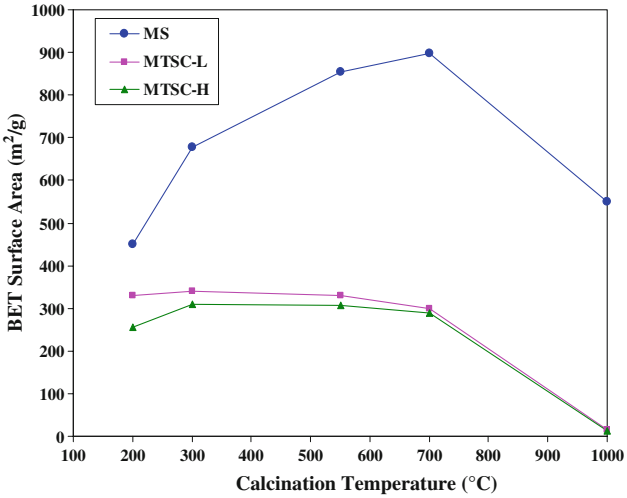

Fig. 7 The variation of BET surface area (for MS, MTSC-L, and MTSC-H) with calcination temperature

H4 hysteresis loops; the two branches remained nearly horizontal and parallel over a wide range of P/P_0 values, indicating the presence of narrow slit-like pores (Fig. 6). The PSDs of MTSC and MS are provided in the supporting information. Generally, the pore diameters tend to widen (increase) with the increase in calcination temperature and the CTAB concentration. For instance, MTSC-3H shows a broader PSD compared to MTSC-3L; and MTSC-2H is considerably wider than MTSC-2L. The as-synthesized samples (MTSC-1L and MTSC-1H) show inferior PSD. As depicted in Fig. 7, the BET surface areas decrease at higher temperature (1000 °C).

Bulk elemental analysis; XRF

The bulk elemental analysis was done using XRF technique. As anticipated, the elements existing in MTSC were O, Si, and Ti. The XRF results indicate that Ti is incorporated into the silica network when titanium oxychloride is used as a Ti source and the overall final ratio of Ti:Si = 2:3. The results obtained using XRF were highly congruent with those obtained using EDS, as shown in Table 1 and in the supporting information.

Table 1 Percentages of Si and Ti in MTSC calcined at various temperatures (results obtained using EDS and XRF techniques)

Sample	Calcination temperature, °C	Si-EDS (%)	Si-XRF (%)	Ti-EDS (%)	Ti-XRF (%)
MTSC-1	Asyn	57.5	61	42.5	39
MTSC-2	550	60	60	40	40
MTSC-3	700	63	60.35	37	39.65
MTSC-4	1000	58	60.8	42	39.2

Discussion

The synthesis route proposed in this study (one-pot co-condensation) is also referred to as the direct functionalization method. It involves the copolymerization of precursors (sodium silicate and titania oxychloride) in the presence of a templating agent. Since the reacting components are incorporated during the condensation of their frameworks, the one-pot co-condensation method might have some superior properties, in applications such as heterogeneous catalysis, compared to our currently reported findings on the titania–silica composite prepared via a grafting method [23]. In one-pot co-condensation route, the composite constituents are likely to be fully integrated into the final product in a controllable loading. Also, it has the advantage of simplicity (fewer synthesis steps) compared to the grafting method [23]. The major disadvantages of the one-pot co-condensation method are poor mesoporosity [as evidenced using nitrogen physisorption studies, low-angle XRD (inset in Fig. 3), and TEM result] and lower titania loadings (as depicted in Table 1; Ti:Si = 2:3 based on EDS and XRF results).

The existing literature reports that the critical micelle concentration (CMC) of CTAB is 0.03 wt% [7]. Above the CMC, a transition from spherical micelles to rod-like micelles occurs, and the size of micelles increases with an increasing concentration of CTAB, eventually resulting in long, rod-like micelles. Despite the considerable number of studies that have been performed to determine the mechanism of formation of templated MS [24–27], the actual mechanism is still unclear [28–30]. The proposed models are neither exclusive nor definitive, in part because essentially the same mesoporous material can be obtained using significantly different reaction conditions. In addition, the physicochemical factors underlying these diverse chemical syntheses have remained obscure due, in large part, to the complicated nature of the multicomponent mixtures and the frequent overlap of the self-assembly and inorganic polymerization processes. These observations were made and then empirically substantiated by Vautier-Giongo and Pastore [31].

In this study, the significant difference in morphologies of samples from Experiments A and B can be explained by considering the flocculating agents generated during the reactions. Because the formation of silicate around surfactant micelles is influenced by both hydrolysis and condensation (to provide charged silica oligomers able to interact with CTA^+ ions and to avoid large particle growth), Na^+ ions must play some role given that we used sodium silicate as the silica source. Hydrolysis of sodium silicate by 2 N HCl generates sodium ions and surfactant (CTA^+) cations, which both act as flocculating agents. Because CTAB is almost completely consumed during micelle formation, the concentration of free CTA^+ is very low in experiment set L. Thus, coagulation that favors the condensation among mesoporous nanoparticles is induced only by Na^+ ions. In contrast, when the initial concentration of CTAB is comparatively high (1.7 wt%), the available charged oligomers of silica will match with the surfactant aggregates and both Na^+ and CTA^+ ions will be available as flocculating agents. In this case, small nuclei would disappear and only large submicrometer-scale primary particles would develop. The mechanism suggested in the present report should be regarded as complementary to those proposed in previous reports, given that the literature provides sufficient evidence that models to explain the origins of MS materials are neither exclusive nor definitive, and are clearly dependent on the nature and concentration of surfactant as well as the silica source.

This observation is compatible with a previous report of a similar experiment based on a sol–gel process using titanium alkoxide as the titania precursor [8]. The products obtained through both experiment sets L and H show similar XRD patterns. Generally, the crystallite sizes increased with an increase in calcination temperature. The average crystallite size D of MTSC-3L and MTSC-4L was calculated using the Debye–Scherrer formula and found to be 4 and 10.1 nm (for the rutile phase) and 4 and 13.4 nm (for the anatase phase), respectively. The anatase phase was transformed to the rutile phase when the calcination temperature was higher than 700 °C; the peak at 27.5° became much sharper owing to further crystallization during the rutile phase. With increasing calcination temperature, the peak intensity of anatase increased, and the width of the (101) peak became narrower. This is due to the growth of anatase crystallites and the enhancement of crystallization. From 700 to 1000 °C, there was an obvious increase in crystal size due to phase transformation from anatase to rutile as a result of the heat provided to accelerate grain growth. The phase transformation temperature of the composite is, however, higher than that of pure titania particles [32]. This is ascribed to the stabilization of the amorphous and anatase TiO_2 phase by the surrounding SiO_2 phase through the Ti–O-Si interface. At the interface, the SiO_2 lattice locks the Ti–O species at the interface of the TiO_2 domains, preventing the nucleation that is necessary for the phase transformation to rutile. Hence, greater heat is required to drive the crystallization [33, 34].

Generally, the weight loss patterns for both experiment set L and H samples were similar, though more weight loss was observed in set H samples due to the higher amount of CTAB (1.7 wt%) used to prepared this sample set compared to set L samples (0.085 wt%). Above 540 °C, composites maintained their weight up to the maximum temperature in this study (1000 °C). This result shows that the mesoporous titania–silica composites developed in this

study have high thermal stability. The pore sizes of the set L samples are in the range of 40–43 Å. The largest BET surface area obtained (for set L samples) was 340 m^2/g, while the total pore volume was 0.42 cm^3/g. In contrast, the pore sizes of the set H samples fell within the range of 52–74 Å. The largest BET surface area obtained was 308 m^2/g, while the total pore volume was 0.53 cm^3/g. BET and BJH results for the samples calcined at 1000 °C (MTSC-L and H) showed the absence of mesopores. This may be due to structural collapse at higher temperatures. There was no appreciable difference in the BET surface area for experimental set L and H samples. Nevertheless, the pore diameters and pore volumes of the experimental set H samples were higher than those of set L, indicating that the amount of template used affects the properties of the final product. Thus, experiment set H samples (prepared at 1.7 wt% CTAB) have more desirable properties, namely, submicrometer-scale morphology, more accessible pores, and a relatively large pore volume.

It was previously pointed out that pore size calculations to determine the mesopore size distribution can be performed on both the adsorption and desorption branches of the isotherm [35]. In the presence of mesopores, capillary condensation will occur during adsorption and is preceded by a metastable fluid state ("cylindrical meniscus"), while capillary evaporation during desorption occurs via a hemispherical meniscus, separating the vapor and the capillary condensed phase. This will result in hysteresis, because pores of a specific size are filled at higher pressures and emptied at lower pressures. If the material under investigation is purely mesoporous and contains nonintersecting mesopores of cylindrical geometry and similar size, the N_2 isotherm will be of type IV accompanied by a type H1 hysteresis loop, according to the IUPAC classification [22]. Both from a historical and thermodynamic point of view, the desorption branch in these cases is most often used to derive the mesopore size distributions from the isotherm ([35] and references therein). In this study, therefore, we used the desorption branch for PSD analysis as demonstrated in the supporting information.

However, closer consideration of the mesoporous titania–silica composites (MTSC-L and H) revealed a more random distribution of pores and an interconnected pore system, and hysteresis loops of Type H2 or H3. In this case, the PSD derived from the desorption branch is often much more affected by pore network effects than the adsorption branch; thus, the adsorption branch may provide a more accurate average PSD (consider the supporting information and the inset therein). Moreover, the hysteresis loops portrayed did not differ significantly between MTSC samples, indicating that the increase in size of anatase TiO_2 nanocrystals at higher calcination temperatures (as evidenced by XRD) did not completely block the pore openings. However, as the calcination temperature increased, the BET surface area gradually decreased (Fig. 7) from the maximum values attained at calcination temperatures of 550 and 700 °C for MSTC and MS, respectively. The lower BET surface area observed in MTSC (compared to MS) is due to the presence of Ti in the silica network; the further decrease at higher calcination temperatures can be attributed to grain growth from the phase transformation of anatase to rutile. The threshold temperature was about 1000 °C. After calcination at this temperature, the BET surface area of all samples decreased drastically, indicating collapse of the mesostructure.

Conclusions

In this paper, we reported a versatile and reproducible route to synthesize mesoporous titania–silica composite using freshly prepared $TiOCl_2$ solution and sodium silicate as a titania and silica precursor, respectively. CTAB surfactant was used as structure-directing agent. FE-SEM, EDS, XRF, XRD, DTGA, and nitrogen physisorption studies revealed the formation of materials with the desired properties, namely, large primary particles (up to 750 nm long and 200 nm wide), highly pure TiO_2–SiO_2 composites with elevated thermal stability (up to 900 °C), large surface area (above 308 m^2/g), easily accessible pores, and adequate pore volume. The FT-IR peak at 954 cm^{-1} confirms the formation of Si–O–Ti bonds in the samples. The experiment set H samples (prepared at 1.7 wt% CTAB) might be considered to have more desirable properties than the set L samples because the set H samples had primary particles sizes in the submicrometer range. The samples prepared by this procedure may potentially be applied in wastewater treatment or as heterogeneous catalysts.

Acknowledgements We would like to thank the Ministry of Commerce and Industries of the Republic of Korea for financial support under the R & D Innovation Fund for Small and Medium Business Administration (Project Application No. S1017370).

References

1. Stokke JM, Mazyck DW (2008) Environ Sci Technol 42:3808
2. Song X, Gao L (2007) J Phys Chem C 111:8180
3. Galindo IR, Viveros T, Chadwick D (2007) Ind Eng Chem Res 46:1138
4. Wang J, Kuhn J, Lu X (1995) J Non-Cryst Solids 186:296–300
5. Mdoe JEG, Macquarrie DJ (2005) Int J Sci Res 14:23
6. Mitrikas G (1998) J Non-Cryst Solids 224:17–22
7. Delsannti M, Moussaid A, Munch JP (1993) J Colloid Interf Sci 157:285
8. Reiche MA, Ortelli E, Baiker A (1999) Appl Catal B 23:187

9. Nishikida K, Iwamoto R (1986) The analysis of material by infrared spectroscopy. Kodansya, Tokyo, p 209
10. Kim JM, Stucky GD (2000) Chem Commun 1159–1160
11. Barrett EP, Joyner LG, Halenda PP (1951) J Am Chem Soc 73:373
12. Pesquera C, González F, Blanco C, Sanchez L (2004) Appl Surf Sci 238:320
13. Sierra L, Guth JL (1999) Microp Mesop Mater 27:243
14. Matos JR, Mercuri LP, Kruk M, Jaroniec M (2002) Langmuir 18:884
15. Zaki MI, Vielhaber B, KnOzinger H (1986) J Phys Chem 90:3176
16. Yu JC, Yu J, Zhao J (2002) Appl Catal B Environ 36:31
17. Lee JH, Yang YS (2005) J Mater Sci 40:2843. doi:10.1007/s10853-005-2434-5
18. Shen S, Deng Y, Zhu G, Mao D, Wang Y, Wu G, Li J, Liu X, Lu G, Zhao D (2007) J Mater Sci 42:7057. doi:10.1007/s10853-007-1608-8
19. Wang HN, Yuan P, Zhou L, Guo YN, Zou J, Yu AM, Lu GQ, Yu CZ (2009) J Mater Sci 44:6484. doi:10.1007/s10853-009-3578-5
20. Berube F, Kleitz F, Kaliaguine S (2009) J Mater Sci 44:6727. doi:10.1007/s10853-009-3566-9
21. Gao X, Wachs IE (1999) Catal Today 51:233
22. Sing KSW, Everett DH, Haul RAW, Moscou L, Pierotti RA, Rouquerol J, Siemieniewska T (1985) Pure App Chem 57(4):603–619
23. Hilonga A, Kim JK, Sarawade PB, Kim HT (in press) J Mater Sci. doi:10.1007/s10853-009-4076-5
24. Kresge CT, Leonowicz ME, Roth WJ, Vartuli JC, Beck JS (1992) Nature 359:710
25. Linden M, Schunck SA, Schüth F (1998) Angew Chem Int Ed Engl 37:82
26. Sicard L, Frasch J, Soulard M, Lebeau B, Patarin J, Davey T, Zana R, Kolenda F (2001) Microp Mesop Mater 44–45:25
27. Zhang J, Carl PJ, Zimmermann H, Goldfarb D (2002) J Phys Chem B 106:5382
28. Ying JY, Mehert CP, Wong MS (1998) Angew Chem Int Ed Engl 37:82
29. Sicard L, Lebeau B, Patarin J, Zana R (2002) Langmuir 18:74
30. Patarin J, Lebeau B, Zana R (2002) Curr Opin Colloid Interf Sci 7:107
31. Vautier-Giongo C, Pastore HO (2006) J Colloid Interf Sci 299:874
32. Khalil KMS, Zaki MI (1997) Powder Technol 92:233
33. Zhao L, Yu J, Chen B (2005) J Solid State Chem 178:1818
34. Yu JG, Yu HG, Cheng B, Zhao XJ, Yu JC, Ho WK (2003) J Phys Chem B 107:13871
35. Groen JC, Peffer LAA, Perez-Ramirez J (2003) Micropor Mesopor Mater 60(1–3):1